catalysts

MDPI

Article

Clean Syngas and Hydrogen Co-Production by Gasification and Chemical Looping Hydrogen Process Using MgO-Doped Fe_2O_3 as Redox Material

Maria Paola Bracciale, Martina Damizia *, Paolo De Filippis and Benedetta de Caprariis

Department of Chemical Engineering Materials and Environment, SAPIENZA University of Rome, Via Eudossiana 18, 00184 Rome, Italy
* Correspondence: martina.damizia@uniroma1.it

Abstract: Gasification converts biomass into syngas; however, severe cleaning processes are necessary due to the presence of tars, particulates and contaminants. The aim of this work is to propose a cleaning method system based on tar physical adsorption coupled with the production of pure H_2 via a chemical looping process. Three fixed-bed reactors with a double-layer bed (NiO/Al_2O_3 and Fe-based particles) working in three different steps were used. First, NiO/Al_2O_3 is used to adsorb tar from syngas (300 °C); then, the adsorbed tar undergoes partial oxidization by NiO/Al_2O_3 to produce CO and H_2 used for iron oxide reduction. In the third step, the reduced iron is oxidized with steam to produce pure H_2 and to restore iron oxides. A double-layer fixed-bed reactor was fed alternatively by guaiacol and as tar model compounds, air and water were used. High-thermal-stability particles 60 wt% Fe_2O_3/40 wt% MgO synthetized by the coprecipitation method were used as Fe-based particles in six cycle tests. The adsorption efficiency of the NiO/Al_2O_3 bed is 98% and the gas phase formed is able to partially reduce iron, favoring the reduction kinetics. The efficiency of the process related to the H_2 production after the first cycle is 35% and the amount of CO is less than 10 ppm.

Keywords: hydrogen; gasification; syngas; chemical looping

Citation: Bracciale, M.P.; Damizia, M.; De Filippis, P.; de Caprariis, B. Clean Syngas and Hydrogen Co-Production by Gasification and Chemical Looping Hydrogen Process Using MgO-Doped Fe_2O_3 as Redox Material. *Catalysts* **2022**, *12*, 1273. https://doi.org/10.3390/catal12101273

Academic Editor: Valerie Dupont

Received: 19 September 2022
Accepted: 17 October 2022
Published: 19 October 2022

1. Introduction

Syngas is a gaseous mixture, mainly composed of hydrogen and carbon monoxide and by small amounts of carbon dioxide and water. The H_2/CO mixture can be produced by gasification of coal/heavy hydrocarbons/biomass and by steam reforming of light hydrocarbons. Syngas is one of the most important intermediates in the chemical industry, mainly used for ammonia, methanol and hydrogen production but also for heat and electricity generation [1–3]. Due to the concerns about global warming and the need to switch to renewable fuels and chemicals, the use of biomass for syngas production is deeply studied. During gasification, biomass is converted into syngas in the presence of an oxidizer (air or oxygen) and a gasifying agent, usually water vapor. The process is composed of four steps: drying, pyrolysis, oxidation and reduction [2]. During the pyrolysis step, occurring at temperatures between 300 and 700 °C, the biomass is decomposed, producing char, gas and vapors, which compose the tar. Part of the produced tar exits from the gasification reactor along with the syngas and can condense in the downstream equipment of the plant, causing clogging of pipes and filters. When the amount of tar exiting from the gasifier is not negligible, for example, when up-draft gasifiers are used, the recovery of the energy of tar by means of its transformation into syngas is fundamental. Tar is a complex mixture of condensable organics, which are generally assumed to be largely aromatic organic species [3,4]. Typically, one- or two-ring aromatic hydrocarbons, including benzene, guaiacol, toluene and naphthalene, are chosen as tar model compounds to deeply investigate the performance of the several tar removal methods [5,6]. The traditional

chemical methods for tar removal are thermal cracking and catalytic reforming; thermal cracking converts tar into syngas and coke at high temperature (T > 800 °C) in the absence of a catalyst; catalytic reforming takes place in the presence of a catalyst, usually Ni, and tar is converted mainly into syngas. These two methods suffer from low conversion efficiency and rapid catalyst deactivation [7].

In this context, chemical looping technologies can represent a viable alternative to remove tar from the syngas and enrich it with H_2. Among them, chemical looping gasification (CLG) and chemical looping reforming (CLR) have attracted a lot of attention from researchers to improve the efficiency and solve the issues related to tar production [8–10]. The process consists of exploiting the redox properties of transition metal oxides in redox cycles. In the first step of the redox cycle, the lattice oxygen of the metal is able to partially oxidizes biomass or tar to syngas, converting the metal oxide into its metallic state. The second step is dedicated to the restoration of the metal oxide using air oxidation to begin the cycle again [11,12]. Huang et al. utilized $NiFe_2O_4$ as oxygen carrier to remove toluene as tar model compound from syngas. The tests showed a high toluene conversion (95%) at 850 °C and also a high stability of the material, which guaranteed a stable conversion after 82 cycles. They also reported the production of a syngas with high H_2 yields [13]. Zeng et al. studied the conversion of naphthalene as tar model compounds over different metal oxides, showing that at 900 °C, more than 90% of naphthalene is converted into CO, CO_2, H_2 and char when CuO, NiO and Fe_2O_3 are used as oxygen carriers [14]. The concept of chemical looping hydrogen (CLH) is slightly different, the first step in tar oxidation/reduction of the metal oxides is comparable to that of chemical looping gasification, but the second step, in which the metal oxide is restored, utilizes water vapor instead of air as the oxidation agent with the goal of pure H_2 production. CLH is widely studied for the production of pure H_2 from renewable sources; however, its application in gasification technology is limited [15]. The most investigated reduction species, needed for the first step of the process, are methane, syngas and ethanol [16,17]. When hydrogen with high purity is required, the use of heavy organic reductants in the CLH process is not common since heavy molecules tend to undergo cracking reactions, forming carbon, which is deposited on the oxygen carrier; the carbon, in the subsequent steps of oxidation, can react with the steam to form CO, undermining the purity of the H_2 stream. To overcome the issues related to carbon formation when heavy-molecular-weight reductants are used, some authors proposed the insertion of a third step of air combustion with the aim of burning the carbon deposited and completely restoring the oxides. Wei et al. investigated the production of H_2 using vegetable oils as reductants and Fe_2O_3 as oxygen carrier. The H_2 stream obtained was composed of H_2 at 90% using a three-step CLH [18]. Xiao et al. also studied a CLH process using bio-oil as reductant and an iron-based oxygen carrier; they worked at 950 °C and obtained an H_2 stream but not pure due to the carbon deposition in the reduction step [19].

The aim of this work is to demonstrate the feasibility of coupling biomass gasification to CLH technology in order to remove tar from the syngas and to produce, at the same time, a pure H_2 stream. The goal is to enhance the whole process efficiency by converting the tar into pure hydrogen, which can be used to enrich the syngas or, as it is, in other applications. With this process, it will be possible to easily produce H_2 from biomass without the need of separation processes of H_2 from syngas. One of the most interesting destinations of pure H_2 is in fuel cell applications, where the CO concentration should be lower than 10 ppm [20].

The experimental study reported in this work is focused only on the tar removal system that consists of one reactor with a double-layer fixed bed, working in three different process steps (tar adsorption, tar partial oxidation and pure hydrogen production). The double layer in each reactor is composed of NiO/Al_2O_3 needed to adsorb the tar and to catalyze tar partial oxidation and by Fe-based particles (60 wt% Fe_2O_3/40 wt% MgO), which constitute the CLH redox system [21]. The catalytic activity of Ni in its oxidized form is proven by numerous studies [22,23]. The process consists of three steps: First,

guaiacol, used as a tar model compound, is adsorbed mainly on the NiO/Al_2O_3 layer at low temperature (300 °C). In the second step, the adsorbed tar is partially oxidized at 700 °C by air, producing heat and syngas. This step is fundamental to convert the adsorbed guaiacol into CO and H_2 needed to reduce iron oxides to iron and to provide the heat needed for iron oxide reduction reactions, favored at high temperature (700–900 °C). In the third step, steam is fed to the reactor in order to produce pure H_2 by iron oxidation and to restore iron oxide. The experimental tests were conducted, studying separately the three steps, looking at the guaiacol abatement efficiency, purity and amount of the produced hydrogen and stability of the oxygen carrier (60 wt% Fe_2O_3-40 wt% MgO).

2. Experimental Section

2.1. Materials

Nitrate salts supplied by Sigma Aldrich (Rome, IT) are used as received for Fe-based particle synthesis (Iron nitrate nonahydrate ($Fe(NO_3)_3 \cdot 9H_2O$), Magnesium nitrate hexahydrate ($Mg(NO_3)_2 \cdot 6H_2O$) and Nickel nitrate nonahydrate ($Ni(NO_3)_2 \cdot 9H_2O$)). A solution of 37 wt% of NaOH is used as precipitation agent. Aluminum oxide powder (Al_2O_3) is supplied by Sigma Aldrich (assay > 99.99%;150 < dp < 300 μm; SSA: 212 $m^2 \cdot g^{-1}$). Guaiacol ($C_7H_8O_2$) was used as tar model compound and used as received by Sigma Aldrich.

2.2. NiO/Al_2O_3 and Fe-Based Particle Syntheses

NiO/Al_2O_3 catalyst with NiO loading of 10 wt% is synthetized by wet impregnation method. The Nickel nitrate solution is prepared by dissolving the calculated amount of nickel salt into distilled water and then the Al_2O_3 particles are added to the solution, then the mixture is heated to allow water evaporation to occur. The obtained particles are calcined in an air static furnace at 800 °C for 4 h.

The Fe-based particles are prepared by coprecipitation method. The calculated amounts of precursor nitrate salts are dissolved into deionized water, then the solution is mixed and heated at 80 °C on a hot plate; when a setting temperature of 80 °C is reached, 37% of NaOH is gradually added to the solution to increase the pH until 11. The solution is aged for 12 h at ambient temperature. The precipitate is filtered and dried at 100 °C overnight. The solid obtained is calcinated in an air-muffle furnace at 350 °C for 2 h and 900 °C for 2 h. Finally, the solid is crushed and sieved to obtain particles in a range of 150 < dp < 300 μm.

2.3. Material Characterization

X-ray powder diffraction (XRD) is implemented to study the crystal-phase compositions before and after the tests for the Fe-based particle. XRD patterns are acquired using a Philips Analytical PW1830 X-ray diffractometer (Malvern, UK), equipped with a Ni β-filtered Cu Kα (1.5418 Å) radiation, in the 2θ range from 5 to 90° with a step size of 0.02° and a time for step of 3.5 s. The data were collected with an acceleration voltage and applied current of 40 kV and 30 mA, respectively. The crystalline phases in the resulting diffractograms were identified through the COD database [24]. The average crystallite size was calculated with the Scherrer's equation on the most intense hkl plane of each detected phase [25].

BET surface area was determined by N_2 adsorption–desorption isotherms acquired at −196 °C using a Micromeritics Triflex analyzer (Micromeritics Instrument Corp., Norcross, GA, USA). The adsorption–desorption isotherms are acquired in a p/p^0 range from 0.01 to 0.99. Isotherm analysis is performed using the 3Flex Version 4.05 software. Samples were previously outgassed at 300 °C for 4 h. The BET equation is used to determine the specific surface area. A morphologic investigation of samples was performed using a High-Resolution-Field Emission Scanning Electron Microscope (HR-FESEM, AURIGA Zeiss, Milan, IT).

2.4. Experimental Set-Up and Procedure

The experiments are conducted in a stainless-steel tubular reactor (di = 1 cm and L = 30 cm) loaded with two fixed-bed layers, having the same dimensions (1 cm height); the first is composed of NiO/Al_2O_3 and the second layer of Fe-based particles. Figure 1 reports a simplified scheme of the plant used for the experiments.

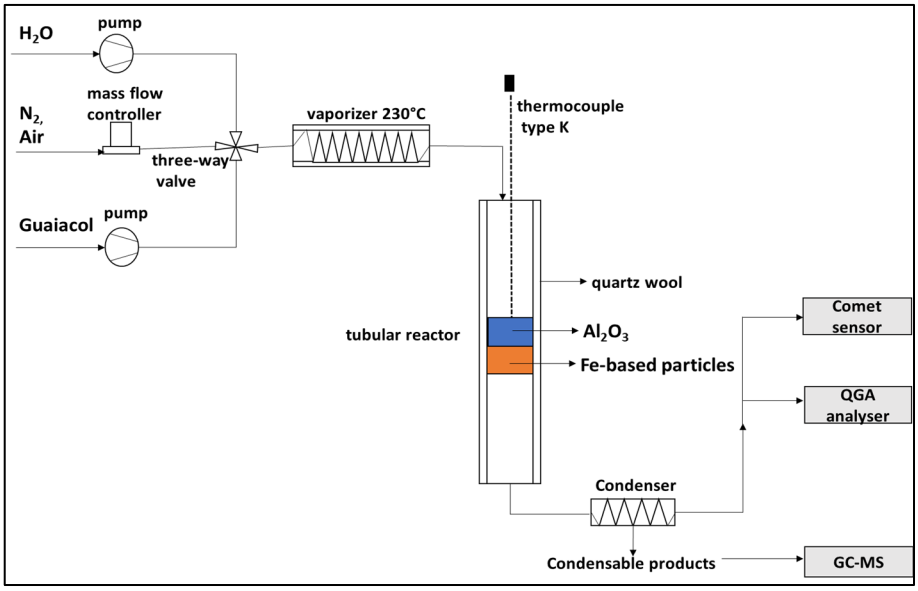

Figure 1. Experimental set-up.

Two syringe pumps are used to feed guaiacol and water, which pass through a vaporizer before entering the reactor. The experimental tests are conducted in the presence of nitrogen as carrier gas (100 mL·min^{-1}) and at atmospheric pressure. The reactor is heated by an external tubular resistance controlled by a K-type thermocouple. The air and nitrogen flow rates are controlled by flow meters. The guaiacol, water and air flow rates are constant and equal to 0.01 mL·min^{-1}, 0.067 mL·h^{-1} and 40 mL·min^{-1}, respectively. The guaiacol flow rate is chosen in order to have an amount of guaiacol in the N_2 that is similar to the amount of tar exiting along with the syngas from an up-draft gasifier (100 mg/Nm^{-3}) [26]. Further, in the adsorption step, which is the first phase of the process, temperature was set to the typical exit temperature of a syngas from an up-draft gasifier (300 °C). In the second and third steps the temperatures are higher and equal to 700 °C. During the adsorption test, the guaiacol stream is forced to pass through 2 g of NiO/Al_2O_3 catalyst. The adsorption tests are performed feeding different amounts of guaiacol, which, at constant guaiacol flow rate, corresponds to different feeding times (15 min, 30 min and 40 min) in order to find the maximum amount of guaiacol that can be adsorbed on the NiO/Al_2O_3. The abatement efficiency was calculated weighing the amount of guaiacol condensed in the flask and the NiO/Al_2O_3 before and after the tests. The guaiacol partial combustion tests are conducted loading the reactor only with NiO/Al_2O_3 bed in order to evaluate the catalyst activity in guaiacol partial oxidation. The amount of air must be carefully controlled since if residual oxygen is present at the exit of the NiO/Al_2O_3 layer it can oxidize the Fe oxides, which are being reduced by the products of partial oxidation of adsorbed guaiacol. At the end of the guaiacol partial-combustion step, the Fe-based particles are reduced and steam is fed to the reactor to start the third step of the process. The gaseous products are analyzed online by mass spectrometer (QGA, Quantitative Gas analyzer) while the liquid product collected in the condenser is analyzed by GC-MS (Agilent 5973, Agilent Technologies, Milan, IT). CO concentration is measured by a non-dispersive infrared sensor (Ambra Sistemi, Comet, Grugliasco, Italy).

3. Discussion

3.1. Characterization of the NiO/Al_2O_3 and Fe-Based Particles

The synthesized materials were characterized to determine their crystallinity and surface area using XRD and BET, respectively.

As shown in Figure 2, the main crystal structures detected in the NiO/Al_2O_3 catalyst are bunsenite (NiO) and corundum (γ-Al_2O_3). No signals associated with the nickel aluminate ($NiAl_2O_4$) spinel phase were detected, which suggests no solid solution among γ-Al_2O_3 and NiO.

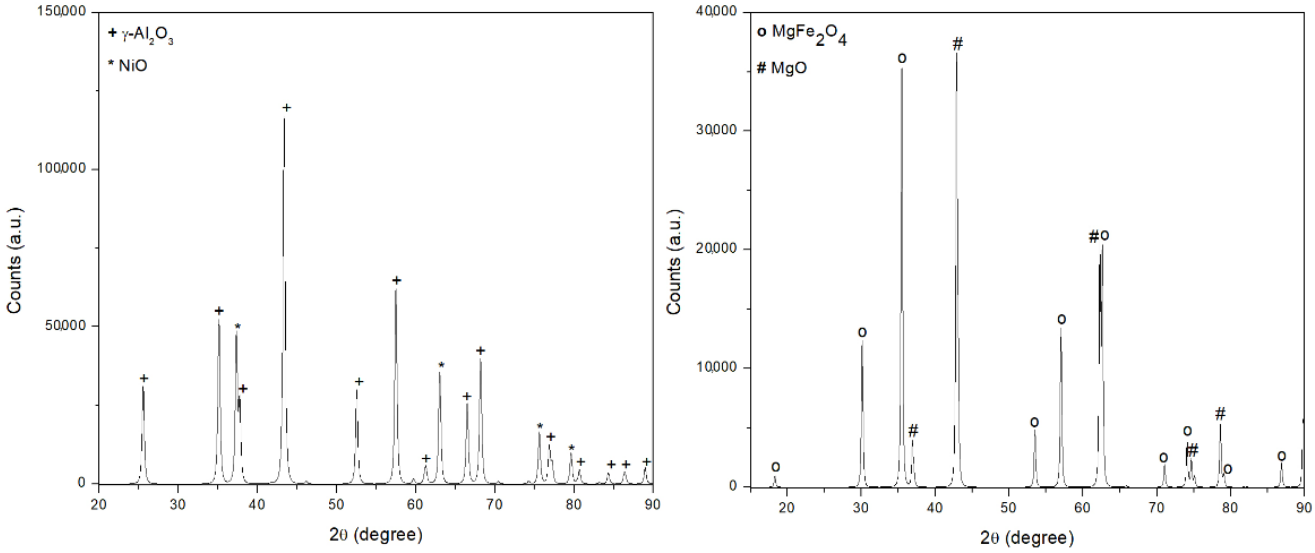

Figure 2. Diffractograms of NiO/Al_2O_3 and 60 wt% Fe_2O_3/40 wt% MgO particles.

The strong interaction between Fe_2O_3 and MgO is instead detected in the case of the 60 wt% Fe_2O_3/40 wt% MgO sample; after calcination in air at 900 °C, magnesium oxide and iron oxide form a spinel structure magnesium ferrite ($MgFe_2O_4$). The specific surface areas (BET) together with pore width and pore volume are presented in Table 1. The NiO/Al_2O_3 catalyst showed a relatively high surface area (196.63 $m^2 \cdot g^{-1}$), but a slight reduction compared with that of the γ-Al_2O_3 support (212 $m^2 \cdot g^{-1}$) occurred, probably due to the presence of NiO particles that partially block the porous network of the support. On the contrary, the Fe-based sample presented lower surface area (9.67 $m^2 \cdot g^{-1}$) and a very low porosity (0.04 $cm^3 \cdot g^{-1}$) compared to the NiO/Al_2O_3 catalyst (0.40 $cm^3 \cdot g^{-1}$).

Table 1. Textural properties.

	NiO/Al_2O_3	**60 wt% Fe_2O_3/40 wt% MgO**
Specific Surface area ($m^2 \cdot g^{-1}$)	195.63 ± 0.04	9.67 ± 0.05
Mean pore width (nm)	9.10	14.08
Total pore volume ($cm^3 \cdot g^{-1}$)	0.40	0.04
Crystal size (nm) [a]	NiO: 49.6; Al_2O_3: 43.9	$MgFe_2O_4$: 97.8; MgO: 87.8

[a] By XRD using Scherrer equation.

3.2. Low-Temperature Guaiacol Adsorption on NiO/Al_2O_3 Particles

In order to evaluate the feasibility to use NiO/Al_2O_3 for the guaiacol adsorption at the operative conditions adopted, tests feeding different amounts of guaiacol (1.365 mmol, 2.731 mmol, 4.095 mmol) are conducted. The flow rate of guaiacol was kept constant at 0.01 $mL \cdot min^{-1}$ and, thus, to feed the different amounts, only the feeding time was changed from 15 to 45 min. The experiments are performed with only the NiO/Al_2O_3 layer in order to better understand the behavior of this material in the process.

At these operative conditions, guaiacol does not undergo any type of decomposition reaction [27]. Therefore, the adsorption efficiency is calculated according to Equation (1):

$$AE(\%) = \frac{Guaiacol\ injected - Guaiacol\ liquid\ product}{Guaiacol\ injected} \times 100 \quad (1)$$

where *guaiacol liquid product* corresponds to the amount of guaiacol collected by condensation at the reactor exit. Table 2 reports the abatement efficiency calculated for each amount of guaiacol fed.

Table 2. Guaiacol abatement efficiency as a function of amount of guaiacol fed with NiO/Al_2O_3 at 300 °C.

Guaiacol Fed (mmol)	Guaiacol in the Condensable Product (mmol)	Abatement Efficiency (%)
1.365	0.020 ± 0.002	98.53
2.731	0.045 ± 0.006	98.35
4.095	2.53 ± 0.023	38.22

As reported in Table 2, guaiacol can be successfully absorbed on NiO/Al_2O_3 at a temperature of 300 °C; however, the time of the adsorption should be carefully tuned and it is a function of the amount of tar into the syngas. The amount of guaiacol in the condensed product at the end of the reactor starts to appear, feeding an amount of guaiacol higher than 2.731 mmol, which corresponds to a feeding time equal to 30 min. For higher feeding time, the abatement efficiency significantly decreases, meaning that the guaiacol is not adsorbed anymore and it is entirely collected as a condensable product. Therefore, the maximum amount of guaiacol that can be adsorbed by the NiO/Al_2O_3 layer is 2.731 mmol.

In order to evaluate if the Fe-based particle layer is involved in the guaiacol adsorption, adsorption experiments are also conducted in the two-layer fixed-bed configuration at the same operative conditions. Table 3 summarizes the results obtained.

Table 3. Guaiacol abatement efficiency as a function of amount of guaiacol fed with double layer (NiO/Al_2O_3+Fe-based particles) at 300 °C.

Guaiacol Fed (mmol)	Guaiacol in the Condensable Product (mmol)	Abatement Efficiency (%)
1.365	0.010 ± 0.003	99.26
2.731	0.025 ± 0.006	99.08
4.095	2.12 ± 0.017	48.82

From the comparison of the results obtained with and without the Fe-based particle layer, it seems that only a slight improvement in the guaiacol abatement efficiency is obtained in the layer of Fe-based particles. These results suggest that the Fe-based particles have a little capacity for adsorption; in fact, only a small amount of the guaiacol fed can be adsorbed on the Fe-based particle layer. From the results, the abatement efficiency of the Fe-based particles is almost negligible due to the very low surface area of this material (9.67 $m^2 \cdot g^{-1}$) compared to that of NiO/Al_2O_3 (195.63 $m^2 \cdot g^{-1}$).

The adsorption of guaiacol into the Fe-based particles is a key aspect that needs to be carefully addressed; in fact, when the temperatures increase during the reduction step, the amount of guaiacol adsorbed onto the Fe-based particles could undergo cracking reactions and form solid carbon on the Fe-based particles, causing deactivation of the active sites. Furthermore, the carbon can react with water vapor in the oxidation steps, producing CO via the gasification reaction. From these considerations, it is clear that the adsorption of guaiacol into the Fe-based particles must be avoided and for the reduction/oxidation tests, the amount of guaiacol that does not imply its adsorption also in the Fe layer is taken as the

optimum amount. The tests of reduction/oxidation were, thus, performed feeding guaiacol for 30 min.

3.3. Guaiacol Partial Oxidation

After the determination of the maximum amount of guaiacol adsorbed by NiO/Al_2O_3 layer, guaiacol partial oxidation experiments are conducted in order to verify the feasibility to partially oxidize guaiacol to form mainly H_2, CO and CO_2. The resulting syngas mixture is used to reduce iron oxides to iron. The experiments are conducted using the configuration in which only the NiO/Al_2O_3 layer is present in order to separately study the partial oxidation of guaiacol and the iron oxide reduction, to measure the amount of heat supplied to the fixed bed by the exothermic partial oxidation reactions [28]. The amount of air fed should be carefully calculated in order to avoid the complete combustion of the adsorbed guaiacol, resulting in the production of CO_2 and H_2O, which could not contribute to iron oxide reduction. Furthermore, oxygen needed for the combustion must be totally consumed by the guaiacol oxidation rection, as its presence at the end of the Al_2O_3 layer hinders the iron oxide reduction. Before starting the partial oxidation step, the reactor is preheated to 700 °C.

The required air flow rate is calculated starting from the maximum amount of guaiacol that can be adsorbed on the NiO/Al_2O_3 layers determined in the previous process step. According to the stoichiometry of guaiacol combustion reaction (reaction (2)), the amount of air required to obtain a complete guaiacol oxidation in 30 min is equal to 80 $mL \cdot min^{-1}$.

$$C_7H_8O_2 + 8O_2 \rightarrow 7CO_2 + 4H_2O \quad (2)$$

Considering that the aim is to partially oxidize guaiacol into CO and H_2, the air flow rate is halved and fixed to 40 $mL \cdot min^{-1}$.

Figure 3 reports the variation in the main compounds detected in the gas phase (H_2, CO, CO_2 and O_2) and the temperature profile of the fixed bed during the test.

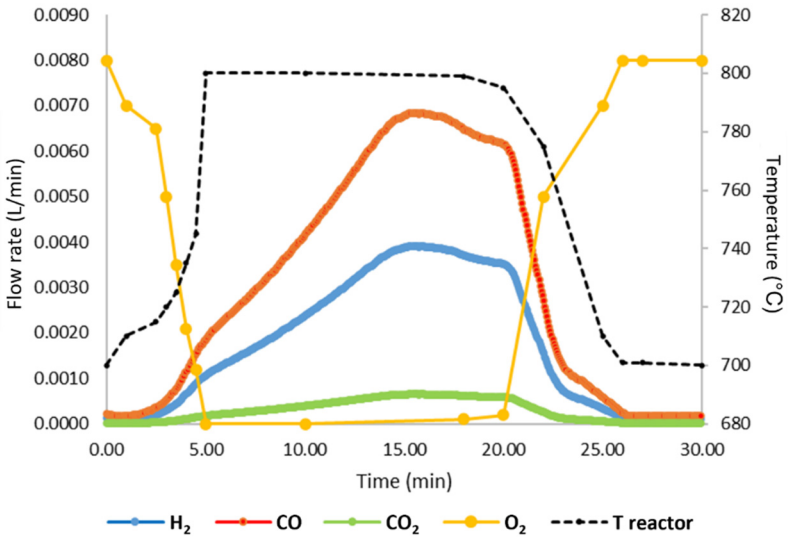

Figure 3. Flow rates of compounds detected in the gaseous phase in the presence of only NiO/Al_2O_3 bed.

As reported in Figure 3, by feeding 40 $mL \cdot min^{-1}$ of air, it is possible to obtain a high reducing power gaseous stream, mainly constituted of CO and H_2, and low amounts of CO_2. The oxygen is totally consumed and is not present in the exiting gases for the first 15 min; after this time, it begins to be revealed, meaning that almost all the guaiacol was consumed. A significant increase in the reactor temperature from 700 to 800 °C is reached thanks the high exothermic nature of the combustion reactions. This additional heat led to an increase in the reaction temperature, promoting kinetics of the iron oxide reduction,

especially with solid carbon, if present. During this step, in fact, solid carbon can be deposited on the Fe-based particle layer since, when the NiO/Al_2O_3 bed with guaiacol adsorbed is heated, part of the guaiacol can be desorbed and flow with the gas phase can undergo cracking reactions, causing the deposition of carbon on the Fe-based particles; the presence of this carbon in order to produce pure H_2 in oxidation should be completely consumed by reduction reactions in order to avoid its presence in the oxidation step, in which it can reacts to give CO, undermining H2 purity. The main reactions taking place in the reduction step are reported below (reactions (3)–(14)) [29].

$$3Fe_2O_3 + H_2 \rightleftarrows 2Fe_3O_4 + H_2O \quad (3)$$

$$Fe_3O_4 + H_2 \rightleftarrows 3FeO + H_2O \quad (4)$$

$$FeO + H_2 \rightleftarrows Fe + H_2O \quad (5)$$

$$3Fe_2O_3 + CO \rightleftarrows 2Fe_3O_4 + CO_2 \quad (6)$$

$$Fe_3O_4 + CO \rightleftarrows 3FeO + CO_2 \quad (7)$$

$$FeO + CO \rightleftarrows Fe + CO_2 \quad (8)$$

$$3Fe_2O_3 + C \rightleftarrows 2Fe_3O_4 + CO \quad (9)$$

$$Fe_3O_4 + C \rightleftarrows 3FeO + CO \quad (10)$$

$$FeO + C \rightleftarrows Fe + CO \quad (11)$$

$$6Fe_2O_3 + C \rightleftarrows 4Fe_3O_4 + CO_2 \quad (12)$$

$$2Fe_3O_4 + C \rightleftarrows 6FeO + CO_2 \quad (13)$$

$$2FeO + C \rightleftarrows 2Fe + CO_2 \quad (14)$$

3.4. Steam Oxidation for Pure H_2 Production

The last step of the process consists of the steam oxidation of the reduced iron oxides at 700 °C. The goal of this step is to oxidize the reduced Fe in order to produce pure H_2 by water splitting according to the reactions (15)–(17) [30].

$$3Fe + 4H_2O \rightleftarrows Fe_3O_4 + 4H_2 \qquad \Delta H < 0 \quad (15)$$

$$3FeO + H_2O \rightleftarrows Fe_3O_4 + H_2 \qquad \Delta H < 0 \quad (16)$$

$$Fe + H_2O \rightleftarrows FeO + H_2 \qquad \Delta H < 0 \quad (17)$$

The oxidation with water vapor is not able to completely restore the Fe to Fe_2O_3; therefore, during this step, Fe_3O_4 is produced [31].

This step is, therefore, conducted with a double-layer (NiO/Al_2O_3+Fe-based particles) fixed bed. Figure 4 shows the flow rates of the main compounds (H_2, CO, CO_2) detected in the gaseous phase in the three steps of the process.

The results reported in Figure 4 demonstrate the feasibility to reduce iron oxide using the gas stream generated by the partial oxidation of the guaiacol adsorbed on NiO/Al_2O_3 particles. In the oxidation step, the hydrogen produced is pure, meaning that in the first cycle, carbon-based compounds are not present or, if present, the carbon is in a form that cannot be easily oxidized by water at the operating conditions adopted. To evaluate the reduction degree of iron oxides during the partial oxidation step, the steam oxidation efficiency (E%) is calculated according to Equation (18):

$$E\ (\%) = \frac{V_{H2}(measured)}{V_{H2}(theoretical)} \times 100 \quad (18)$$

where V_{H2} is the volume of H_2 obtained during the steam oxidation step and $V_{H2\ theoretical}$ is the maximum amount of H_2 producible, considering the total reduction of iron oxides to metallic iron and the total oxidation of Fe to Fe_3O_4. The calculated steam oxidation efficiency is equal to 35%. The results suggest that the complete reduction to metallic iron is not reached and that the amount of reducing agents produced from partial guaiacol oxidation are not sufficient to achieve the complete iron oxide reduction at the operating condition adopted. However, the produced H_2 has high purity (CO < 10 ppm) and, thus, it can be utilized in a large variety of applications (Automotive, chemical industry).

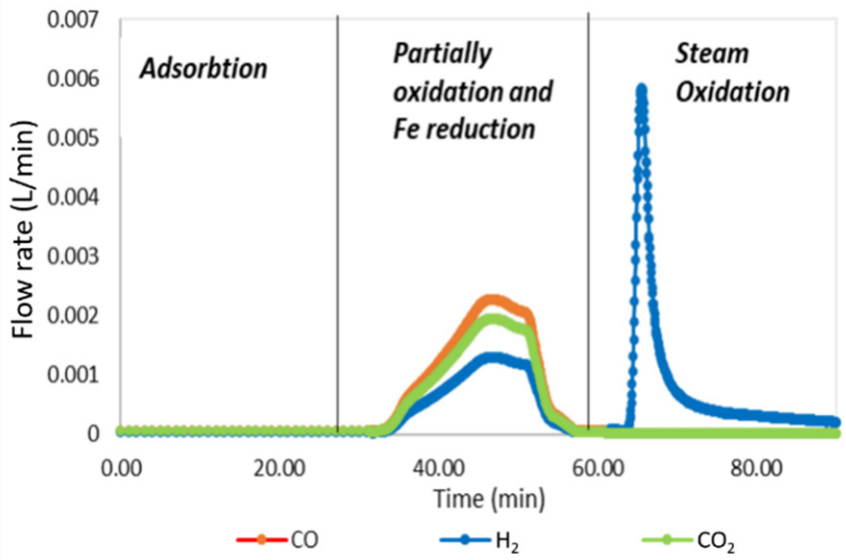

Figure 4. Flow rates of the main compounds detected in the gaseous phase in the 3-step system with double-layer fixed bed.

3.5. Stability Test

To evaluate the feasibility of the process and the resistance of the Fe-based particles, a test with six cycles is conducted. Each cycle includes the guaiacol adsorption, guaiacol partial oxidation and Fe reduction and oxidation by water vapor. The results of the stability tests in terms of process efficiency and hydrogen purity are reported in Figure 5.

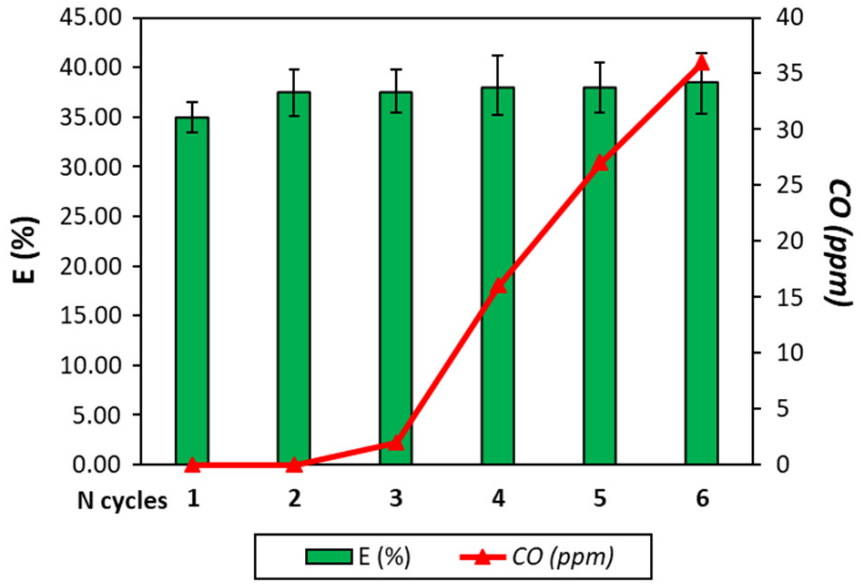

Figure 5. Stability tests, process efficiency and CO concentration in the H_2 stream.

As already said, the efficiency of the first cycle is 35% and an increase in the efficiency to 38% is registered. This phenomenon was expected since, after the first cycle, the Fe-based particles in oxidation form are composed of Fe_3O_4 and, thus, a lower amount of reducing gases is needed to reach metallic Fe. However, the efficiency is still low, meaning that the reducing form of the particle is not Fe. The efficiency is stable for the six cycles, meaning that the synthetized 60 wt% Fe_2O_3/40 wt% MgO particles possess good thermal stability. The addition of MgO to Fe_2O_3 increases the resistance of Fe_2O_3 to high temperature [32]. However, after three cycles, CO begins to be produced, undermining the H_2 purity, and after the third cycle, the CO concentration overtakes the limit of 10 ppm if the H_2 must be used for fuel cell application, for example. This result suggests that in the Fe particle bed, carbon is present and its amount tends to increase cycle after cycle.

To solve this issue and to guarantee the H_2 purity, the six-cycle test is repeated but after the third cycle, a diluted air flow (oxygen concentration 10%) is fed to the reactor in order to burn all the carbon deposited. The regeneration step lasts 7 min, until the CO_2 concentration falls to 0. The results are reported in Figure 6 and, as expected, the hydrogen purity in this way is guaranteed. In this way, the CO concentration never exceeds 10 ppm.

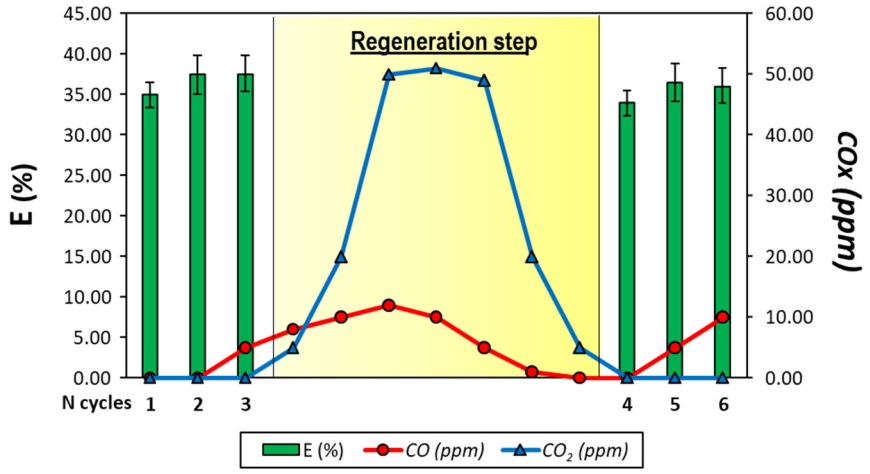

Figure 6. Stability tests; process efficiency and CO, CO_2 concentration in the H_2 stream and during the combustion step.

As can be seen from Table 4, the feasibility to remove tar from syngas by chemical looping technologies was already demonstrated. However, the data reported highlight that the use of a chemical looping hydrogen process can maximize the tar removal efficiency, obtaining a separated pure H_2 stream.

Table 4. Comparison of literature results and our work.

Process	MeOx	Tar Removal	H_2/CO Syngas	Purity H_2	REF
CLG	Fe_2O_3	90% *	-	-	[14]
CLR	NiO	96%	2.2	-	[33]
CLR	Mn_3O_4-$MgZrO_3$	56%	1	-	[34]
CLG	$NiFe_2O_4$	89%	0.78	-	[35]
CLG + water splitting	$NiFe_2O_4$	80%	2.21	50%	[36]
CLH	Fe_2O_3-MgO	98% *	-	100%	This work

*: Tar Model Compound.

4. Characterization of the Fe-Based Particles after the Three-Step Redox Cycles

XRD analyses are conducted on the synthetized Fe-based articles before and after the three-step tests in order to better understand the behavior of the redox material in the process. As discussed in Section 3.1, a strong interaction between Fe_2O_3 and MgO is detected after calcination in air at 900 °C; magnesium oxide and iron oxide form a spinel structure. Magnesium ferrite ($MgFe_2O_4$), which is one of the most important ferrites that

finds a wide number of applications in heterogeneous catalysis, is observed in the sensor sector and in magnetic technologies [37]. These interactions modify the redox system of the Fe_2O_3 and MgO; in fact, looking at Figure 7, after reduction, iron is reduced in two different structures. Part of the iron is present as magnetite and the other amount forms a mixed oxide, named magnesiowustite $(Mg_{0.6}\ Fe_{0.4})O$ with oxidation state equal to +2. However, no iron signal is detected, confirming the incomplete reduction achieved in the three-step redox cycle test. At the end of the test, the sample is composed of $MgFe_2O_4$ and MgO and, therefore, it can be used in a subsequent cycle. The mean crystallite size calculated from the Scherrer equation is 177.1 nm for the spinel phase and 403.1 nm for MgO.

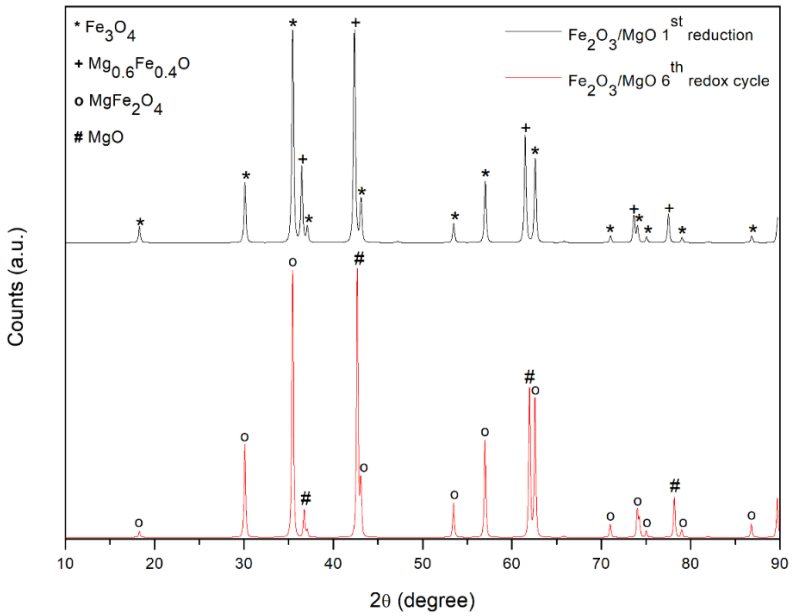

Figure 7. XRD pattern of Fe-based particles after the first reduction step and after the three-step redox cycles.

Looking at the SEM pictures reported in Figure 8, the high thermal stability of this material is confirmed. It can be noted that the dimension of particles suffered a slight increase in size; the crystallites in the sample are clearly visible also after the stability test, meaning that any synthetization phenomenon can occur. This result confirms the positive effect of MgO addition on the activity and stability of iron oxides in the steam iron process.

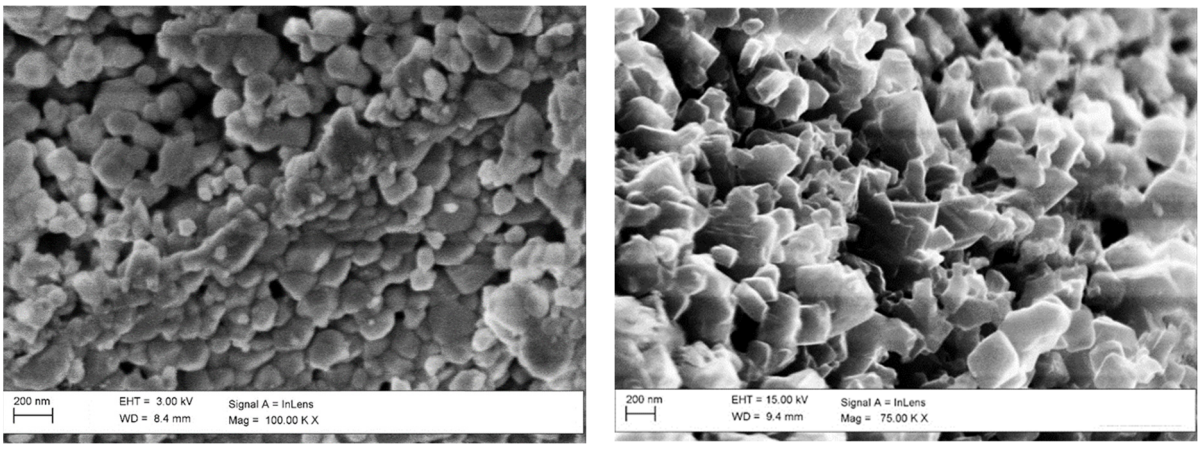

(**a**) (**b**)

Figure 8. SEM pictures of the fresh sample (**a**) and of the sample after the first cycle (**b**).

5. Conclusions

In this work, an innovative syngas cleaning process was studied, demonstrating the feasibility of using tar as a reductant agent for chemical looping hydrogen processes. The aim is to remove tar from syngas, converting it into pure hydrogen. The proposed process consists of three steps (tar adsorption, guaiacol partial oxidation/iron oxide reduction and hydrogen production/iron oxidation) and to demonstrate the efficiency of each step, they were first studied independently. The adsorption efficiency of the NiO/Al_2O_3 bed was 98% when an amount of guaiacol equal to 2.731 mmol was fed. The partial oxidation of guaiacol to produce the iron oxide reducing agents was successfully tested; from the analysis, the iron oxides appeared to be partially reduced and an increase in the bed temperature of 100 °C was detected, favoring the reduction kinetics.

The efficiency of the process related to the hydrogen production after the first cycle was 35% and the amount of CO less than 10 ppm. Stability tests with six cycles were conducted, demonstrating that the synthetized material possesses a great resistance to thermal stability. However, after two cycles, the amount of CO in the produced H_2 stream begins to increase due to the accumulation of unreacted carbon in the Fe particle bed. The introduction of a combustion step in the process, aimed at cleaning the iron-based particles from carbon, was successfully tested, obtaining a continuous production of pure H_2.

The results reported in this study demonstrate that the chemical looping hydrogen process can be a very interesting alternative to recover the energy contained in tar by using it to produce pure hydrogen. In this way, the efficiency and the flexibility of the whole gasification process can be considerably improved; in fact, with this configuration, it is possible to produce clean syngas enriched with hydrogen but also two high-value separated streams: syngas and pure hydrogen, exploitable in a great number of applications.

Author Contributions: Conceptualization, methodology, writing—original draft preparation M.D. and M.P.B.; writing—review and editing and supervision, B.d.C.; funding acquisition, P.D.F. All authors have read and agreed to the published version of the manuscript.

Funding: This research received no external funding.

Data Availability Statement: The data presented in this study are available on request from the corresponding author.

Conflicts of Interest: The authors declare no conflict of interest.

References

1. Ding, L.; Yang, M.; Dong, K.; Vo, D.V.N.; Hungwe, D.; Ye, J.; Ryzhkov, A.; Yoshikawa, K. Mobile Power Generation System Based on Biomass Gasification. *Int. J. Coal Sci. Technol.* **2022**, *9*, 34. [CrossRef]
2. De Filippis, P.; Scarsella, M.; De Caprariis, B.; Uccellari, R. Biomass Gasification Plant and Syngas Clean-up System. *Energy Procedia* **2015**, *75*, 240–245. [CrossRef]
3. Jeong, Y.S.; Mun, T.Y.; Kim, J.S. Two-Stage Gasification of Dried Sewage Sludge: Effects of Gasifying Agent, Bed Material, Gas Cleaning System, and Ni-Coated Distributor on Product Gas Quality. *Renew. Energy* **2022**, *185*, 208–216. [CrossRef]
4. Torres, C.; Rostom, S.; de Lasa, H. An Eco-Friendly Fluidizable FexOy/CaO-γ-Al_2O_3 Catalyst for Tar Cracking during Biomass Gasification. *Catalysts* **2020**, *10*, 806. [CrossRef]
5. Motak, M.; Meng, X.; Zhang, X.; Łamacz, A. Toluene Steam Reforming over Ni/$CeZrO_2$—The Influence of Steam to Carbon Ratio and Contact Time on the Catalyst Performance and Carbon Deposition. *Catalysts* **2022**, *12*, 219. [CrossRef]
6. McFarlan, A.; Maffei, N. Assessing Tar Removal in Biomass Gasification by Steam Reforming over a Commercial Automotive Catalyst. *Fuel* **2018**, *233*, 291–298. [CrossRef]
7. Tian, Y.; Ma, X.; Chen, X.; Zhang, C.; Li, J. The Study of Coke Resistance of Ni/ZrO_2 by Core-Shell Structure Coupling with Cobalt Doping Modification in CO_2 Reforming of Tar. *Appl. Catal. A Gen.* **2022**, *643*, 118797. [CrossRef]
8. Goel, A.; Moghaddam, E.M.; Liu, W.; He, C.; Konttinen, J. Biomass Chemical Looping Gasification for High-Quality Syngas: A Critical Review and Technological Outlooks. *Energy Convers. Manag.* **2022**, *268*, 116020. [CrossRef]
9. Samprón, I.; de Diego, L.F.; García-Labiano, F.; Izquierdo, M.T. Effect of the Fe Content on the Behavior of Synthetic Oxygen Carriers in a 1.5 KW Biomass Chemical Looping Gasification Unit. *Fuel* **2022**, *309*, 122193. [CrossRef]
10. Hoxha, A.; Palone, O.; Cedola, L.; Stendardo, S.; Borello, D. Development of a Novel Carbon Capture and Utilization Approach for Syngas Production Based on a Chemical Looping Cycle. *Fuel* **2022**, *325*, 124760. [CrossRef]

11. Udomsirichakorn, J.; Salam, P.A. Review of Hydrogen-Enriched Gas Production from Steam Gasification of Biomass: The Prospect of CaO-Based Chemical Looping Gasification. *Renew. Sustain. Energy Rev.* **2014**, *30*, 565–579. [CrossRef]
12. Wang, X.; Jin, B.; Liu, H.; Zhang, B.; Zhang, Y. Prediction of In-Situ Gasification Chemical Looping Combustion Effects of Operating Conditions. *Catalysts* **2018**, *8*, 526. [CrossRef]
13. Huang, Z.; Zheng, A.; Deng, Z.; Wei, G.; Zhao, K.; Chen, D.; He, F.; Zhao, Z.; Li, H.; Li, F. In-Situ Removal of Toluene as a Biomass Tar Model Compound Using $NiFe_2O_4$ for Application in Chemical Looping Gasification Oxygen Carrier. *Energy* **2020**, *190*, 116360. [CrossRef]
14. Zeng, J.; Hu, J.; Qiu, Y.; Zhang, S.; Zeng, D.; Xiao, R. Multi-Function of Oxygen Carrier for in-Situ Tar Removal in Chemical Looping Gasification: Naphthalene as a Model Compound. *Appl. Energy* **2019**, *253*, 113502. [CrossRef]
15. Das, S.; Biswas, A.; Tiwary, C.S.; Paliwal, M. Hydrogen Production Using Chemical Looping Technology: A Review with Emphasis on H_2 Yield of Various Oxygen Carriers. *Int. J. Hydrogen Energy* **2022**, *47*, 28322–28352. [CrossRef]
16. Stoppacher, B.; Sterniczky, T.; Bock, S.; Hacker, V. On-Site Production of High-Purity Hydrogen from Raw Biogas with Fixed-Bed Chemical Looping. *Energy Convers. Manag.* **2022**, *268*, 115971. [CrossRef]
17. De Filippis, P.; D'Alvia, L.; Damizia, M.; de Caprariis, B.; Del Prete, Z. Pure Hydrogen Production by Steam-Iron Process: The Synergic Effect of MnO_2 and Fe_2O_3. *Int. J. Energy Res.* **2021**, *45*, 4479–4494. [CrossRef]
18. Wei, G.Q.; Zhao, W.N.; Meng, J.G.; Feng, J.; Li, W.Y.; He, F.; Huang, Z.; Yi, Q.; Du, Z.Y.; Zhao, K.; et al. Hydrogen Production from Vegetable Oil via a Chemical Looping Process with Hematite Oxygen Carriers. *J. Clean. Prod.* **2018**, *200*, 588–597. [CrossRef]
19. Xiao, R.; Zhang, S.; Peng, S.; Shen, D.; Liu, K. Use of Heavy Fraction of Bio-Oil as Fuel for Hydrogen Production in Iron-Based Chemical Looping Process. *Int. J. Hydrogen Energy* **2014**, *39*, 19955–19969. [CrossRef]
20. Baschuk, J.J.; Li, X. Carbon Monoxide Poisoning of Proton Exchange Membrane Fuel Cells. *Int. J. Energy Res.* **2001**, *25*, 695–713. [CrossRef]
21. de Caprariis, B.; Damizia, M.; De Filippis, P.; Bracciale, M.P. The Role of Al_2O_3, MgO and CeO_2 Addition on Steam Iron Process Stability to Produce Pure and Renewable Hydrogen. *Int. J. Hydrogen Energy* **2021**, *46*, 39067–39078. [CrossRef]
22. Kobayashi, Y.; Horiguchi, J.; Kobayashi, S.; Yamazaki, Y.; Omata, K.; Nagao, D.; Konno, M.; Yamada, M. Effect of NiO Content in Mesoporous NiO–Al_2O_3 Catalysts for High Pressure Partial Oxidation of Methane to Syngas. *Appl. Catal. A Gen.* **2011**, *395*, 129–137. [CrossRef]
23. Chu, Y.; Li, S.; Lin, J.; Gu, J.; Yang, Y. Partial Oxidation of Methane to Carbon Monoxide and Hydrogen over NiO/La_2O_3/γ-Al_2O_3 Catalyst. *Appl. Catal. A Gen.* **1996**, *134*, 67–80. [CrossRef]
24. Graulis, S.; Chateigner, D.; Downs, R.T.; Yokochi, A.F.T.; Quirós, M.; Lutterotti, L.; Manakova, E.; Butkus, J.; Moeck, P.; Le Bail, A. Crystallography Open Database—An Open-Access Collection of Crystal Structures. *J. Appl. Crystallogr.* **2009**, *42*, 726–729. [CrossRef] [PubMed]
25. Farrauto, R.J.; Hobson, M.C. Catalyst Characterization. In *Encyclopedia of Physical Science and Technology*; Elsevier: Amsterdam, The Netherlands, 2003; pp. 501–526.
26. Awais, M.; Li, W.; Arshad, A.; Haydar, Z.; Yaqoob, N.; Hussain, S. Evaluating Removal of Tar Contents in Syngas Produced from Downdraft Biomass Gasification System. *Int. J. Green Energy* **2018**, *15*, 724–731. [CrossRef]
27. Furutani, Y.; Dohara, Y.; Kudo, S.; Hayashi, J.I.; Norinaga, K. Theoretical Study on the Kinetics of Thermal Decomposition of Guaiacol and Catechol. *J. Phys. Chem. A* **2017**, *121*, 8495–8503. [CrossRef]
28. Miyazawa, T.; Kimura, T.; Nishikawa, J.; Kado, S.; Kunimori, K.; Tomishige, K. Catalytic Performance of Supported Ni Catalysts in Partial Oxidation and Steam Reforming of Tar Derived from the Pyrolysis of Wood Biomass. *Catal. Today* **2006**, *115*, 254–262. [CrossRef]
29. Heidari, A.; Niknahad, N.; Iljana, M.; Fabritius, T. A Review on the Kinetics of Iron Ore Reduction by Hydrogen. *Materials* **2021**, *14*, 7540. [CrossRef]
30. Stehle, R.C.; Bobek, M.M.; Hooper, R.; Hahn, D.W. Oxidation Reaction Kinetics for the Steam-Iron Process in Support of Hydrogen Production. *Int. J. Hydrogen Energy* **2011**, *36*, 15125–15135. [CrossRef]
31. Bleeker, M.F.; Kersten, S.R.A.; Veringa, H.J. Pure Hydrogen from Pyrolysis Oil Using the Steam-Iron Process. *Catal. Today* **2007**, *127*, 278–290. [CrossRef]
32. Murugan, A.; Thursfield, A.; Metcalfe, I.S. A Chemical Looping Process for Hydrogen Production Using Iron-Containing Perovskites. *Energy Environ. Sci.* **2011**, *4*, 4639–4649. [CrossRef]
33. Berguerand, N.; Lind, F.; Israelsson, M.; Seemann, M.; Biollaz, S.; Thunman, H. Use of Nickel Oxide as a Catalyst for Tar Elimination in a Chemical-Looping Reforming Reactor Operated with Biomass Producer Gas. *Ind. Eng. Chem. Res.* **2012**, *51*, 16610–16616. [CrossRef]
34. Lind, F.; Israelsson, M.; Seemann, M.; Thunman, H. Manganese Oxide as Catalyst for Tar Cleaning of Biomass-Derived Gas. *Biomass Convers. Biorefinery* **2012**, *2*, 133–140. [CrossRef]
35. Fan, Y.; Tippayawong, N.; Wei, G.; Huang, Z.; Zhao, K.; Jiang, L.; Zheng, A.; Zhao, Z.; Li, H. Minimizing Tar Formation Whilst Enhancing Syngas Production by Integrating Biomass Torrefaction Pretreatment with Chemical Looping Gasification. *Appl. Energy* **2020**, *260*, 114315. [CrossRef]

36. He, F.; Huang, Z.; Wei, G.; Zhao, K.; Wang, G.; Kong, X.; Feng, Y.; Tan, H.; Hou, S.; Lv, Y.; et al. Biomass Chemical-Looping Gasification Coupled with Water/CO_2-Splitting Using $NiFe_2O_4$ as an Oxygen Carrier. *Energy Convers. Manag.* **2019**, *201*, 112157. [CrossRef]
37. Maensiri, S.; Sangmanee, M.; Wiengmoon, A. Magnesium Ferrite ($MgFe_2O_4$) Nanostructures Fabricated by Electrospinning. *Nanoscale Res. Lett.* **2009**, *4*, 221–228. [CrossRef]